JOURNAL OF SPACECRAFT AND ROCKETS
Vol. 43, No. 4, July–August 2006

Dynamic Characteristic Formulations for Jointed Space Structures

Tomihiko Yoshida*
Nippon Telegraph and Telephone Corporation, Kanagawa 239-0847, Japan

New mathematical formulations are described for estimating the dynamic characteristics of deployable space structures. The two main effects of the structure joints are transitions in natural frequencies and energy dissipation. These effects are formulated individually by using a nonlinear spring model and friction- and impact-damping models. The total effects of the joints are obtained by integrating the models using energy loss factors. The formulations are quite efficient compared to numerical analyses because the dynamic characteristics can be obtained mathematically for each cycle without time-consuming calculations. Analyses and experimental evaluations show the dynamic characteristics and demonstrate the validity of the formulations.

Nomenclature

A = cross-sectional area in the joint
a = amplitude in the contact condition (maximum deflection of the beam)
b = joint width (clearance width)
C = decrement gradient
E = Young's modulus of the joint
E_{FL} = quarter-cycle energy dissipation caused by friction
$E_{\mathrm{FL}g}$ = quarter-cycle friction loss caused by gravity
E_I = internal energy of the beam
E_{RL} = quarter-cycle energy dissipation caused by impact
e = restitution coefficient of the joint
f = natural frequency of the beam
f_b = shearing stress by friction (friction stress) on bottom surface in the joint
f_u = shearing stress by friction (friction stress) on upper surface in the joint
f_0 = natural frequency in the noncontact condition
f_1 = natural frequency in the contact condition
h = joint height
h_0 = offset between the centroid axis and the neutral axis (zero-strain axis) of the joint (Fig. 6)
I = moment of inertia of area of the joint
k = equivalent stiffness of the beam
k_0 = stiffness in the noncontact condition
k_1 = stiffness in the contact condition
L = beam length
l = effective joint length (clearance length)
M = bending moment in the joint
M_0 = bending moment at $x = 0$
m = mass of the beam
N = shearing force in the joint
n = vertical stress (constricted stress) in the joint
P = external force on the beam
Q = vertical force at $x = l$
q = vertical stress in the joint
R = vertical force at $x = 0$
r = vertical stress in the joint
T = reactive force in the joint
t = time
w = bending deflection
x = horizontal axis, when equal to 0 (y axis) indicates the boundary between the joint and the beam (Fig. 5)
y = vertical axis, when equal to (x axis) indicates the centroid axis of the undeformed beam (Fig. 5)
δ = logarithmic decrement of the beam
ε = half of the clearance thickness
θ_0 = rotating-free angle of the beam
λ_b = slippage displacement on the bottom surface in the joint
λ_u = slippage displacement on the upper surface in the joint
μ = friction coefficient of the joint
ξ = energy loss factor for one cycle
σ = bending stress in the joint

Superscript

i = time index

I. Introduction

RECENTLY, we have begun to use large deployable antennas[1] on satellites to realize broadband mobile satellite services for handheld terminals. To design satellites with large space structures (LSS) that are deployable, such as large antennas, we must estimate the dynamic characteristics of the LSS for accurate controller designs. Because the LSS are difficult to ground test, predictions by analyses that assume the space environment are indispensable. One analysis problem is the impact of the joints in the LSS.[2] Each LSS contains many joints that must have specific clearances to allow smooth deployment at a specific temperature. However, the clearances have strongly nonlinear characteristics, and so traditional linear analysis techniques cannot easily handle the dynamic characteristics.

Prestress is a well-known design technique for eliminating the nonlinear responses of a deployed structure to compress the joints with small constricted stress. Even with this technique, however, the natural frequency and damping characteristics are altered by slippage of the joint surfaces. A bigger problem is that the prestress cannot be used during deployment. It is clear that we need a design methodology that can accurately predict the clearance effects for a deployable structure of reasonable complexity.

Many studies on the clearance effects of these structures have been done.[3–14] However, practical estimation methods are not yet available. In many cases, the joint models are assumed to be spring–viscous damper models to simulate the joints' friction and impact damping,[3–5] or are assumed to be restitution coefficient models that can simulate impact damping.[6,7] However, because the joint effects generally involve frequency and damping transitions,[3,8,9] we would be negligent if we considered only the damping characteristics.

Received 30 January 2005; revision received 11 October 2005; accepted for publication 25 October 2005.

*Engineer, Satellite Communication Service Development Project, Access Network Service Systems Laboratories, Yokosuka, 1-1 Hikarinooka.

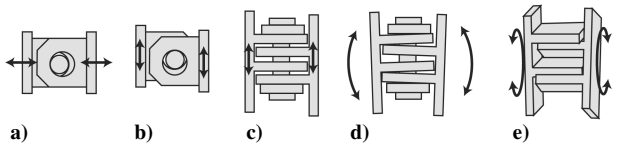

Fig. 1 Clearance of pin-joint.

Some commercial numerical structural analysis software can solve the dynamic structure response with clearances.[10,11] However, they consume a lot of CPU time or cannot solve the analysis model because the calculations can become unstable.

In forced vibration conditions, the joint effects exhibit chaotic behavior and a jumping phenomenon. This chaotic behavior shows that the dynamic response strongly depends on the position and the amplitude of the forced excitation.[6,7,12] The jumping phenomenon is a sudden change in the frequency response.[13] This makes it difficult to estimate the dynamic characteristics of a jointed structure.

In this paper, the author proposes new mathematical formulations that can estimate total joint effects including frequency and damping transitions. The models for the formulations are one-dimensional, single-jointed beams in the primary (low-order) bending mode of free vibration. Higher modes that are induced by impact can be ignored in many cases because they degrade more quickly than low-order modes. Moreover, because space structures are subjected to continuous forced excitation only during launch, a free-vibration model is practicable.

The key feature of the proposed formulation is that the joint model includes a nonlinear spring model and friction- and impact-damping models. The models are integrated using energy-loss factors[14] to estimate both the frequency and damping characteristics without time-consuming calculations; the dynamic characteristics can be obtained immediately. The author proves the applicability of the formulations by analyses and experimental evaluations.

II. Formulations

A. Classification of Clearance Effects

The biggest differences between jointed and nonjointed structures are the transitions in natural frequency and the energy dissipation exhibited by the former.

In linear systems, the pin-joint is considered to have one degree of freedom around the pin. However, the pin-joint must have some clearance to enable smooth rotation, and so that it can move in the other five directions as shown in Figs. 1a–1e. The natural frequency transitions can be explained by considering the contact and noncontact conditions of the clearances. In the contact condition, because the joint cannot move further in the contact direction, the mode shape and natural frequency of the structure are almost the same as in the linear model. In the noncontact condition, the joint is floating within the clearance, so that if the mode shape is different from the linear model the natural frequency will be different. Therefore, a vibrating structure experiences changes in its natural frequency, depending on the contact or noncontact conditions. A free-vibrating structure generally settles into some noncontact configuration because of the energy dissipation caused mainly by friction and impact in the joints and structural damping in the beams.

The following sections show formulations of the joint effects, classified into frequency transition and friction and impact damping. The energy loss factors that denote the ratio of dissipated energies to the total energy are derived to integrate these formulations and to predict the dynamic characteristics.

B. Natural Frequency Transition

In this section, a one-dimensional cantilever with joint support as shown in Fig. 2 is examined. In the contact condition (Fig. 2c), the joint-supported cantilever is assumed to be a fixed-end cantilever. In the noncontact condition (Figs. 2a and 2b), the cantilever behaves as a free-end beam. We can easily see that the mode shape and the natural frequency depend on the condition. Figure 3 shows equivalent mass–spring models that correspond to Fig. 2. The equivalent spring is nonlinear, as shown in Fig. 4.

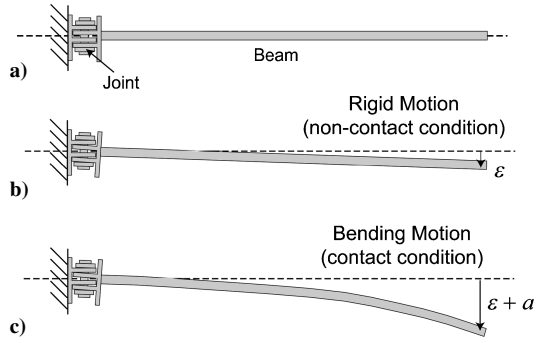

Fig. 2 Joint-supported cantilever.

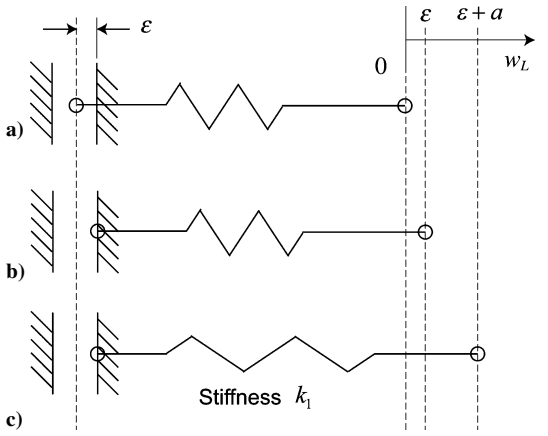

Fig. 3 Equivalent model of joint-supported cantilever.

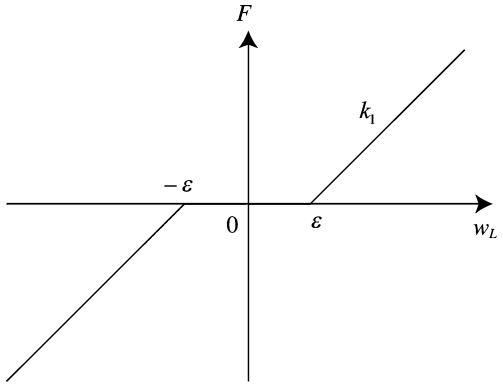

Fig. 4 Nonlinear spring stiffness.

In the contact and noncontact conditions, the equations of motion for the equivalent systems are given as

$$m\ddot{w}_L + k_0 w_L = 0 \qquad (w_L \le \varepsilon)$$

$$m\ddot{w}_L + k_1 w_L = (k_1 - k_0)\varepsilon \qquad (w_L > \varepsilon) \tag{1}$$

where w_L is the equivalent bending deflection at the free-end of the cantilever. Damping terms, such as friction and impact effects, can be ignored in Eq. (1) because the effects on the natural frequency are small.

The natural frequency of the system can be derived from the reciprocal of the time from the state in Fig. 3c to the state in Fig. 3a using Eq. (1), such as

$$f = \frac{\pi}{2}\left\{ f_1 \Big/ \left[\cos^{-1} G + \gamma \tan^{-1}\left(\frac{\gamma G}{\sin\cos^{-1} G} \right) \right] \right\} \tag{2}$$

where γ is the ratio of the frequencies, $\gamma = f_1/f_0$, and $G = (\varepsilon/a)/[(\varepsilon/a) + \gamma^2]$. When a rigid-body motion ($k_0 = 0$, $f_0 = 0$) is considered, Eq. (2) is simplified to

$$f|_{f_0=0} = f_1/[1 + (2/\pi)(\varepsilon/a)] \tag{3}$$

From Eqs. (2) and (3), it is found that the natural frequency transition depends on the ratio of the clearance thickness ε to the amplitude a. It is also confirmed that, when the amplitude in the contact condition is much less than the clearance thickness ($\varepsilon/a \gg 1$), the natural frequency closely approaches the noncontact natural frequency, $f \simeq f_0$, as opposed to $\varepsilon/a \ll 1$, $f \simeq f_1$. In general, the amplitude is degraded by the energy dissipation. Therefore, the natural frequency gradually becomes the noncontact natural frequency.

C. Energy Dissipation Caused by Friction

In this section, the author will calculate the friction energy dissipation in a joint that supports a bending beam. The joint is supposed to be a constricted joint, such as those seen in the prestress condition, and a small-clearance joint, similar to a pin-joint. The joint model is shown in Figs. 5 and 6. The assumptions for the formulations are 1) Euler beam joint, 2) static condition, 3) constant friction coefficient, and 4) zero gravity.

The energy dissipation is caused by slippage in the joint under the influence of the bending moment M_0 that is caused by P. The dissipation is obtained by multiplying the friction force by the contact surface slippage displacement. To derive the friction force and slippage displacement, the author will show the force and moment distributions in the joint.

The force and moment balance equations are given as

$$P = b\int_0^l (r - q)\,\mathrm{d}x$$

$$M_0 = b\int_0^l (-r + q)x\,\mathrm{d}x + \frac{bh}{2}\int_0^l (f_u + f_b)\,\mathrm{d}x \tag{4}$$

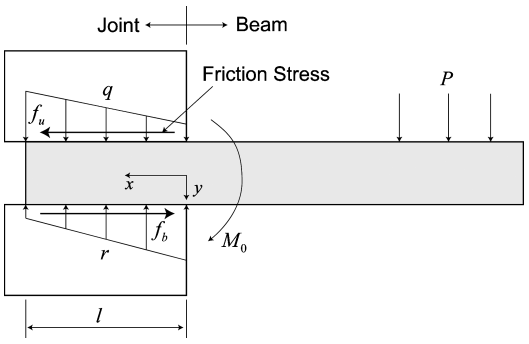

Fig. 5 Joint model.

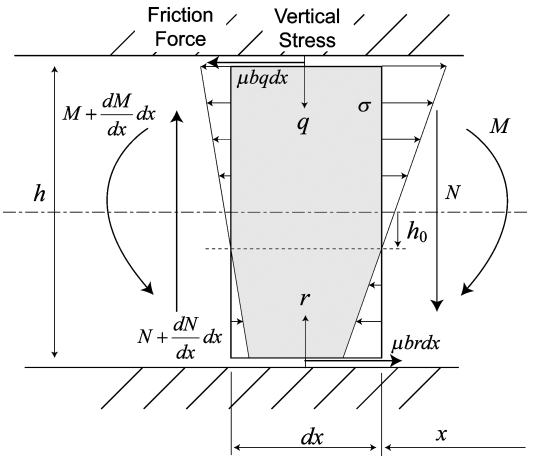

Fig. 6 Small element of joint model.

The vertical stresses r and q and effective joint length l are unknown parameters, and each vertical stress is assumed to include one unknown parameter.

The friction stress for the upper surface is given as

$$f_u = \begin{cases} \sigma_{y=-h/2} & (\sigma_{y=-h/2} < \mu q) \\ \mu q & (\sigma_{y=-h/2} \geq \mu q) \end{cases} \tag{5a}$$

and for the bottom surface as

$$f_b = \begin{cases} -\sigma_{y=h/2} & (-\sigma_{y=h/2} < \mu r) \\ \mu r & (-\sigma_{y=h/2} \geq \mu r) \end{cases} \tag{5b}$$

The bending stress is given as

$$\sigma = -(M/I)(y - h_0) \tag{6}$$

Bending moment M and offset h_0 are derived as follows.

As shown in Fig. 6, the equations for the force balance and moment balance of the small joint element are given as

$$\frac{\mathrm{d}N}{\mathrm{d}x} = b(-r + q), \qquad \frac{\mathrm{d}M}{\mathrm{d}x} = N - \frac{bh}{2}(f_u + f_b) \tag{7}$$

Bending moment M is derived by integrating Eq. (7), with boundary conditions of $N|_{x=0} = P$ and $M|_{x=0} = M_0$.

The horizontal force balance equation is

$$\int \sigma(x)\,\mathrm{d}A + bf_b\,\mathrm{d}x = \int \sigma(x + \mathrm{d}x)\,\mathrm{d}A + bf_u\,\mathrm{d}x \tag{8}$$

Simplifying Eq. (8), we obtain the offset as

$$h_0 = \frac{I}{h}(f_b - f_u)\Big/\left(\frac{\mathrm{d}M}{\mathrm{d}x}\right) \tag{9}$$

The bending deflection of the joint is given as

$$w = \iint \frac{1}{h}\left(\frac{\sigma_{y=-h/2} - f_u}{E} + \frac{-\sigma_{y=h/2} - f_b}{E}\right)\mathrm{d}x\,\mathrm{d}x$$

$$= \iint \left(\frac{M}{EI} - \frac{f_u + f_b}{hE}\right)\mathrm{d}x\,\mathrm{d}x \tag{10}$$

The boundary conditions are assumed to be $w|_{x=l} = 0$ and $(\mathrm{d}w/\mathrm{d}x)|_{x=l} = 0$.

Note that the bending deflection is limited by the joint reactive force T on the contact surface, which depends on the bending deflection, vertical stresses, and so on. Therefore, the reactive force is assumed to be the sum of the vertical forces in the joint, such as

$$T = b\int_0^l (r + q)\,\mathrm{d}x \tag{11}$$

First, using Eqs. (4–11) [mainly Eqs. (4), and (11)], we solve three unknown parameters: the vertical stresses r and q and the effective joint length l. Next, if the obtained effective joint length is larger than the actual joint length, the actual joint length is used as l. In such a case, we can clarify two parameters r and q using Eq. (4).

The energy dissipation can be derived by multiplying the friction force by the surface slippage displacement. The displacement on the upper surface is given by

$$\lambda_u = -\frac{1}{E}\int_l^x (\sigma_{y=-h/2} - f_u)\,\mathrm{d}x \tag{12a}$$

and on the bottom surface by

$$\lambda_b = -\frac{1}{E}\int_l^x (-\sigma_{y=h/2} - f_b)\,\mathrm{d}x \tag{12b}$$

Therefore, the quarter-cycle energy loss caused by friction is derived as

$$E_{\mathrm{FL}} = \int_0^l \mu bq\lambda_u \,\mathrm{d}x + \int_0^l \mu br\lambda_b \,\mathrm{d}x \tag{13}$$

Equation (13) is the energy dissipation model caused by friction.

Because the preceding formulations are somewhat complicated to solve, Eq. (13) was simplified. When the actual joint length is short and the moment M_0 is relatively large, Eq. (5) can be simplified to

$$f_u = \mu q, \qquad f_b = \mu r \tag{14}$$

When the joint is constricted, such as in the prestress conditions, the vertical stress model is assumed as

$$q = q_l + n, \qquad r = r_0 + n \tag{15}$$

where q_l and r_0 are assumed to satisfy

$$\int_{x=l} bq_l \,\mathrm{d}x = Q, \qquad \int_{x\neq l} bq_l \,\mathrm{d}x = 0$$

$$\int_{x=0} br_0 \,\mathrm{d}x = R, \qquad \int_{x\neq 0} br_0 \,\mathrm{d}x = 0$$

The vertical forces Q and R are unknown parameters.

From Eqs. (14) and (15), Eq. (4) becomes

$$P = R - Q$$

$$M_0 = \mu hR/2 + lQ + \mu bhnl \tag{16}$$

Therefore, the vertical forces Q and R are obtained by Eq. (16), such as

$$Q = \frac{M_0 - \mu hP/2 - \mu bhnl}{l + \mu h/2}$$

$$R = \frac{M_0 + lP - \mu bhnl}{l + \mu h/2} \tag{17}$$

From Eq. (7), the moment in the joint is obtained as

$$M = Q(l - x) + \mu bhn(l - x) \tag{18}$$

From Eq. (9), $h_0 = 0$.

From Eq. (10), the bending deflection is calculated as

$$w_0 = \frac{Q + \mu bhn}{EI}\frac{l^3}{6} - \frac{\mu n}{hE}l^2 \tag{19}$$

where w_0 is the bending deflection at $x = 0$. In Sec. III, the reactive force T is assumed to contain a third-order spring,[8] such as

$$T = k_\alpha w_0 + k_\beta w_0 n^3 \tag{20}$$

where k_α and k_β are constant values that can be derived by experimental identification. From Eqs. (11) and (20), the following equation is obtained:

$$T = Q + R + 2nbl = k_\alpha w_0 + k_\beta w_0 n^3 \tag{21}$$

From Eqs. (17) and (21), the effective joint length l is obtained. If the actual joint length is smaller than the obtained effective length, the actual length would be used as l instead of the obtained length.

When Eqs. (14–18) are applied to Eqs. (6) and (12), the slippage displacement on the surface is given as

$$\lambda_u = \lambda_b = \frac{Q + \mu bhn}{EI}\frac{h}{2}\left(\frac{l^2}{2} - lx + \frac{x^2}{2}\right) - \frac{1}{E}\mu n(l - x) \tag{22}$$

The quarter-cycle energy loss is derived by Eqs. (13) and (22) as

$$E_{\mathrm{FL}} = \mu R\left(\frac{Q + \mu bhn}{EI}\frac{hl^2}{4} - \frac{1}{E}\mu nl\right)$$

$$+ 2\mu bn\left(\frac{Q + \mu bhn}{EI}\frac{hl^3}{12} - \frac{1}{E}\mu n\frac{l^2}{2}\right) \tag{23}$$

When external force P and bending moment M_0 are given, the energy loss is easy to calculate using Eq. (23). This simple formulation is a significant benefit. Moreover, when force P is concentrated at the free end of the beam, and the beam length L is longer than the joint length,

$$M_0 = PL, \qquad Q \simeq R \simeq PL/(l + \mu h/2) \tag{24}$$

If the joint is not constricted, $n = 0$, so that Eq. (23) can be simplified as

$$E_{\mathrm{FL}} = \mu hl^2 QR/(4EI) \tag{25}$$

Equation (25) shows the energy dissipation model of the small-clearance joint.

D. Energy Dissipation Caused by Impact

In this section, the energy loss model that accounts for impact is derived. First, to identify the damping characteristics caused by impact, experimental results are presented. Figure 7 shows the time response of free vibration in the experimental model shown in Fig. 8. Figure 7 also shows the result of an analysis model that is a linear mass–spring–viscous damper model. These two envelopes are quite different. We know that the free-vibration amplitude of linear mass–spring–viscous damper systems decreases exponentially. However, the envelope of the experimental model is almost linear. This result shows the linear viscous damper models cannot explain the impact effects.

The author introduces a suitable model that can simulate this linear envelope by using the restitution coefficient. The restitution coefficient is defined as

$$e \equiv (v_{2a} - v_{1a})/(v_{1b} - v_{2b}) \tag{26}$$

where v_{1b} and v_{2b} are velocities before collision and v_{1a} and v_{2a} are velocities after collision.

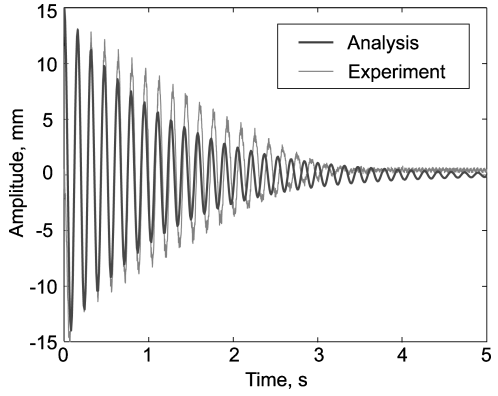

Fig. 7 Time responses of experimental model and linear mass–spring–damper analysis model.

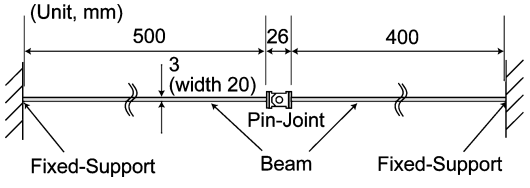

Fig. 8 Experimental model.

Figure 9 shows the simulation model corresponding to Fig. 8. Figure 10 shows the numerical time-simulation result of the model in Fig. 9. In this simulation, the restitution coefficient is assumed to be zero and friction and structural damping are not considered. The fourth-order Runge–Kutta method is applied for the numerical calculations.

It is found that the envelopes for both the simulation and experiment results are linear and similar. Under different conditions, the time responses in the simulations and experiments also show linear envelopes, such that

$$a = -Ct + a_0 \tag{27}$$

We found that the numerical simulation model can describe the impact damping well; however, this simulation is time consuming. Therefore, the envelope gradient C, called the decrement gradient, was used to derive the energy loss caused by impact. The dependencies of the decrement gradient on the joint parameters are clarified by numerical simulations. The joint parameters are assumed to be clearance thickness, impact masses, natural frequencies, and restitution coefficient. The obtained decrement gradients from the time-simulation results are shown in Fig. 11, where m_1 and m_2 are impact masses and f_1 and f_2 are natural frequencies in the noncontact condition on each cantilever. Subscript a indicates a smaller value of subscripts 1 and 2, for instance, m_a is the smaller of m_1 and m_2, whereas subscript b indicates the larger value.

We found that the decrement gradient tends to be linear to the mass ratio, the frequency difference, and clearance thickness and is constant for restitution coefficients between 0 and 0.4, as shown in Fig. 11. Therefore, the decrement gradient is predictable, such that

$$C = \kappa\varepsilon\rho^{\alpha}\left(f_b^{\beta} - f_a^{\beta}\right)^{1/\beta}\gamma_e \tag{28}$$

where κ, α, and β are complementary coefficients, $\rho = m_a/m_b$ ($m_a \le m_b$) is the ratio of mass, and γ_e is a function that depends on restitution coefficient e. In this simulation, $\kappa = 1.5$, $\alpha = 0.35$, and $\beta = 1.3$ were taken as appropriate values.

The quarter-cycle energy dissipation is derived using the decrement gradient. When the amplitude changes from a_1 to a_2 for one cycle, the relationship to the decrement gradient is given by

$$a_1 - a_2 = CT = C/f \tag{29}$$

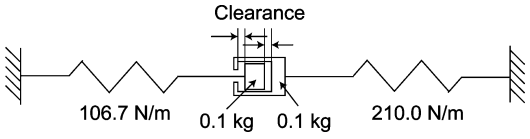

Fig. 9 Equivalent simulation model.

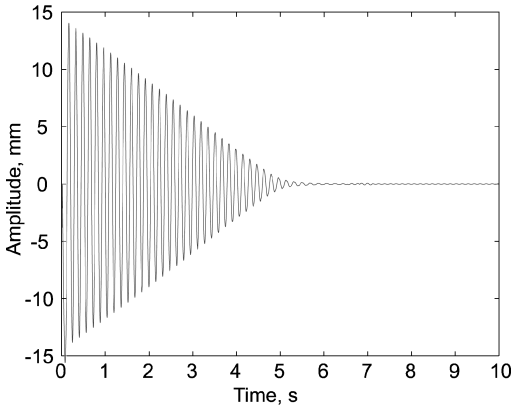

Fig. 10 Time response of simulation model.

where T is the time for one cycle. When the internal energy of the beam is described as

$$E_I = \tfrac{1}{2}ka^2 \tag{30}$$

the one cycle energy loss is given as

$$4E_{\mathrm{RL}} = \tfrac{1}{2}k_1a_1^2 - \tfrac{1}{2}k_2a_2^2 \tag{31}$$

where k_1 and k_2 are the equivalent stiffnesses corresponding to a_1 and a_2, respectively. When the equivalent stiffnesses are almost equal, $k \simeq k_1 \simeq k_2$, the quarter-cycle energy loss is derived as

$$E_{\mathrm{RL}} = kaC/4f \tag{32}$$

where $a = (a_1 + a_2)/2$. Equations (28) and (32) are the energy dissipation models that account for impact.

E. Dynamic Characteristics Estimation

In this section, we will integrate the preceding formulations using the energy loss factor,[14] and we will derive the logarithmic decrement and time-frequency characteristics as the dynamic characteristics. Because the characteristics are obtained mathematically on each cycle, the estimation is extremely fast and efficient.

The energy loss factor is defined as the ratio of the energy dissipation to the total energy for one cycle, given as

$$\xi \equiv 4(E_{\mathrm{FL}} + E_{\mathrm{RL}})/E_I \tag{33}$$

where the energy dissipation caused by friction E_{FL} is given by Eqs. (23) or (25) and the energy dissipation caused by impact E_{RL} is given in Eq. (32).

The energy loss factor is also described by using Eq. (30):

$$\xi = 1 - \left(ka_1^2/2\right)/\left(ka_0^2/2\right) = 1 - (a_1/a_0)^2 \tag{34}$$

therefore,

$$a_1 = \sqrt{1-\xi}\,a_0 \tag{35}$$

The logarithmic decrement is defined as

$$\delta \equiv \log(a_0/a_1) \simeq 1 - (a_1/a_0) \tag{36}$$

The dynamic characteristics can be obtained by using the following steps:

1) Clearance thickness ε, initial amplitude a_0, and frequency in the noncontact and contact conditions f_0 and f_1 are set.

2) From Eq. (2), we obtain the natural frequency f^i using ε, a^{i-1}, f_0, and f_1. The present time is given as $t^i = t^{i-1} + 1/f^i$.

3) We obtain the next amplitude a^i using Eqs. (33) and (35). The logarithmic decrement is given by Eq. (36).

4) To obtain the time-frequency analysis, repeat steps 2 and 3.

III. Analyses and Experiments

To confirm the given formulations, analyses and experimental evaluations were carried out.

The experimental setups are shown in Fig. 12. The beam is made of aluminum, $E = 71{,}000$ N/mm^2; its dimensions are given in Fig. 13. Figure 13 shows the configurations of the experimental models. Configuration 1, shown in Figs. 12a and 13a, is the joint-supported cantilever. The joint is used instead of the fixed end. First, the constricted joint, $\sigma = 0.75$ and 1.25 N/mm^2, is applied. Second, the small-clearance joint, $\theta_0 = 0.02$ and 0.01 rad, is used, where θ_0 is the rotating-free angle that corresponds to the clearance thickness ε. Configuration 2, shown in Figs. 12b and 13b, is a beam with both ends fixed. However, it has a pin-joint in the center of the beam. The hole in the diameter of the joint is 8 mm and we used 6-mm ($\varepsilon = 1$ mm) and 7-mm ($\varepsilon = 0.5$ mm)-diam pins.

The logarithmic decrement and time–frequency characteristic experiment results are shown in Figs. 14–16. Figures 14–16 show the averages and error bars of five measurement runs. We can see

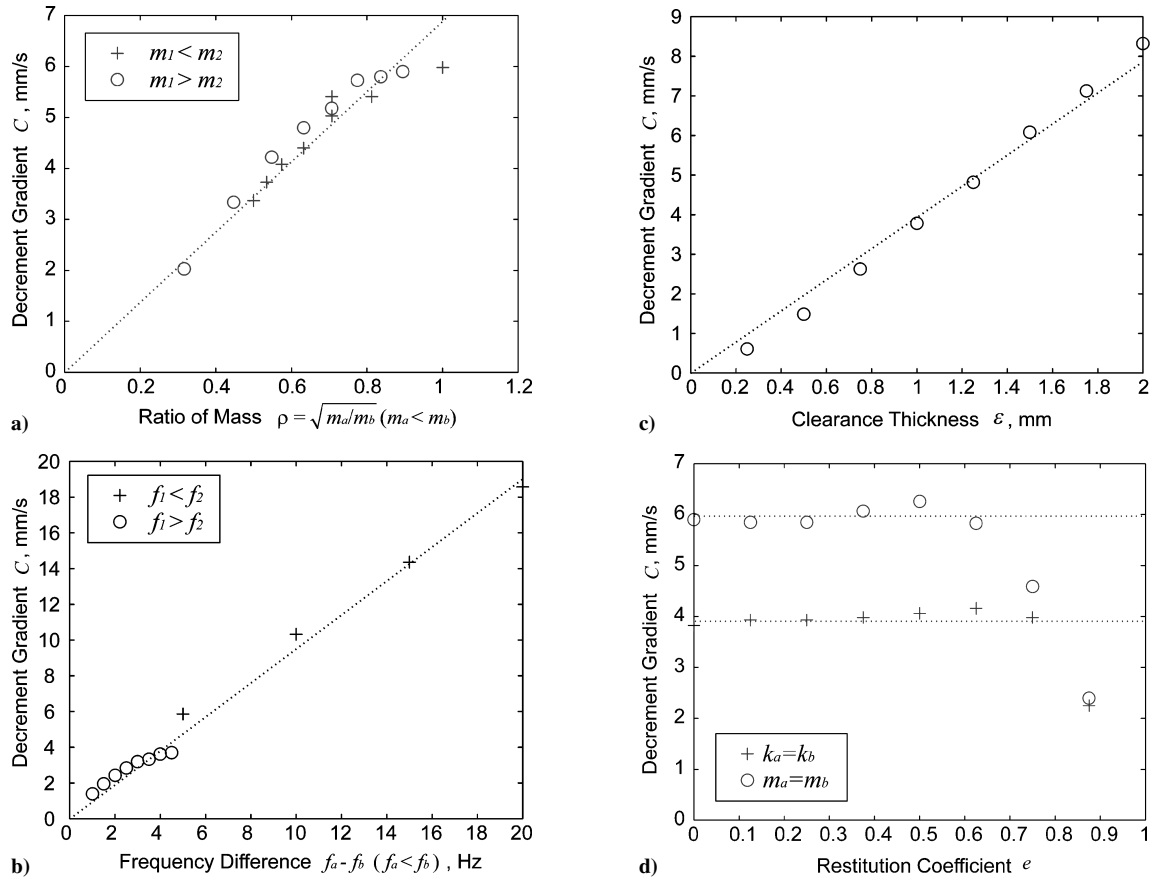

Fig. 11 Decrement gradient dependency on a) mass, b) frequency, c) clearance thickness, and d) restitution coefficient.

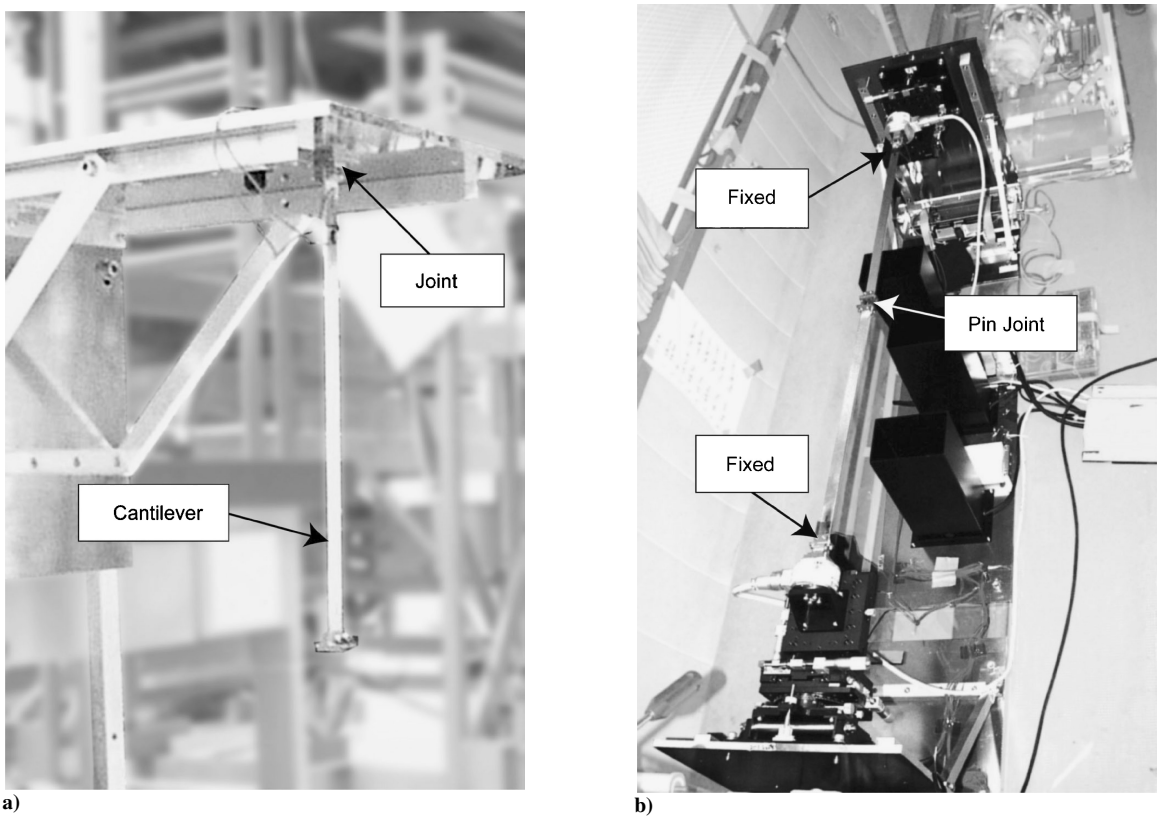

Fig. 12 Experimental setup: a) configuration 1 and b) configuration 2.

that the measurement accuracy is slightly degraded at small amplitudes. The reason is that small amplitude enlarges the nonlinear clearance effects as, described in Sec. II.B. In this case, the measurement error for the logarithmic decrement was about 0.01 and the frequency error was about 0.5 Hz at small amplitudes. On the other hand, measurement accuracy at large amplitudes was high.

In configuration 1, because the joint length is much smaller than the beam length, the velocity before collision in the joint is very small. Therefore, impact damping is negligible. The energy loss factor is mainly caused by friction. Because the beam is set vertically, as shown in Fig. 12a, the friction loss caused by gravity must be considered, such that

$$E_{\mathrm{FL}g} = \mu m g d \theta_0 \tag{37}$$

where g is the gravity acceleration and d is the length from rotation center to the contact point of the joint. This value is static and small because of the small clearance. When the amplitude in the contact condition is very small, the internal energy is very small. In this case, the friction loss by gravity dominates the energy loss factor.

In configuration 2, the friction loss is ignored because the pin-joint does not transmit bending moment to the other beams and the friction dissipation is very small because $M_0 = 0$. Therefore, the energy loss is mainly caused by impact. The natural frequencies in the contact and non-contact conditions are assumed to be the same because the mode shapes are almost the same as mentioned in Sec. II.A. Therefore, we can apply $f = f_0 = f_1$ as shown in Eq. (2).

Equations (3) and (23) are applied to the constricted joint cantilever; Eqs. (3), (25), and (37) are applied to the small clearance joint cantilever; and Eq. (32) is applied to configuration 2. Also, the structural damping is considered in the analyses. From Eqs. (34–36), the energy loss factor due to the structural damping, ξ_{SL}, can be obtained from the logarithmic decrement of the free-vibrating fixed-end cantilever, δ_{SL}, such that $\xi_{\mathrm{SL}} = 1 - (1 - \delta_{\mathrm{SL}})^2$, and ξ_{SL} is added to right-hand side of Eq. (33). Because δ_{SL} was about 0.01 in a preliminary experiment, this value is used in the equation.

The results using the proposed mathematical formulations described in Sec. II.E are also shown in Figs. 14–16. The computation time to obtain both the logarithmic decrement and time–frequency characteristics was a few seconds for each configuration. Therefore, this analysis can estimate the dynamic characteristics very rapidly.

Figure 14 shows the analysis and experimental results for the cantilever with constricted joint support. Both results are very close to each other. In particular, the logarithmic decrement at $\sigma = 1.25$ N/mm^2 shows a complex dependency on amplitude. Our analysis predicts this complex dependency very well.

Figure 15 shows the results for the cantilever with the small-clearance joint support. We found that the logarithmic decrement increased rapidly at small amplitudes and frequency declined quickly over time. The analysis predicted these dynamic characteristics very well.

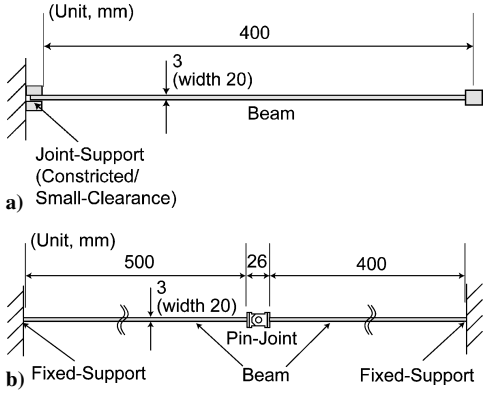

Fig. 13 Configurations for experiment: a) configuration 1 and b) configuration 2.

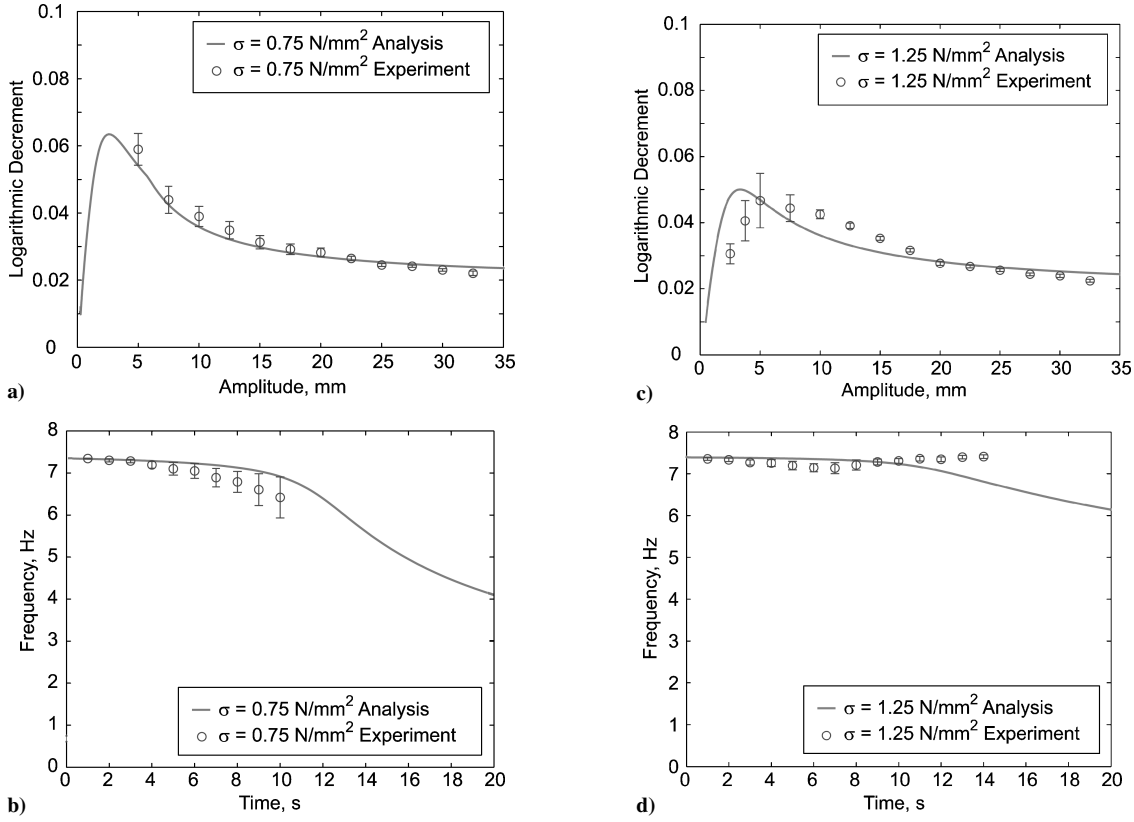

Fig. 14 Dynamic characteristics of cantilever with constricted joint support: a) logarithmic decrement, $\sigma = 0.75$ N/mm^2; b) time–frequency characteristics $\sigma = 0.75$ N/mm^2; c) logarithmic decrement, $\sigma = 1.25$ N/mm^2; and d) time–frequency characteristics, $\sigma = 1.25$ N/mm^2.

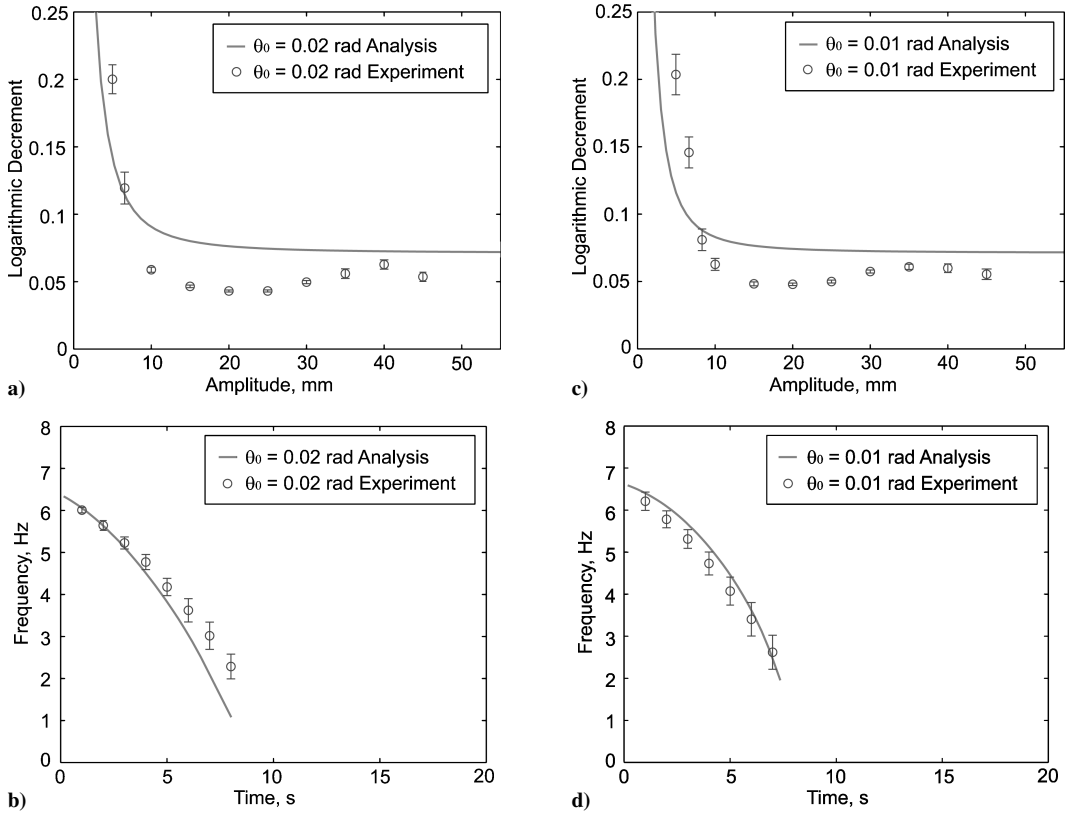

Fig. 15 Dynamic characteristics of cantilever with small-clearance joint support: a) logarithmic decrement, $\theta_0 = 0.02$ rad; b) time–frequency characteristics, $\theta_0 = 0.02$ rad; c) logarithmic decrement, $\theta_0 = 0.01$ rad; and d) time–frequency characteristics, $\theta_0 = 0.01$ rad.

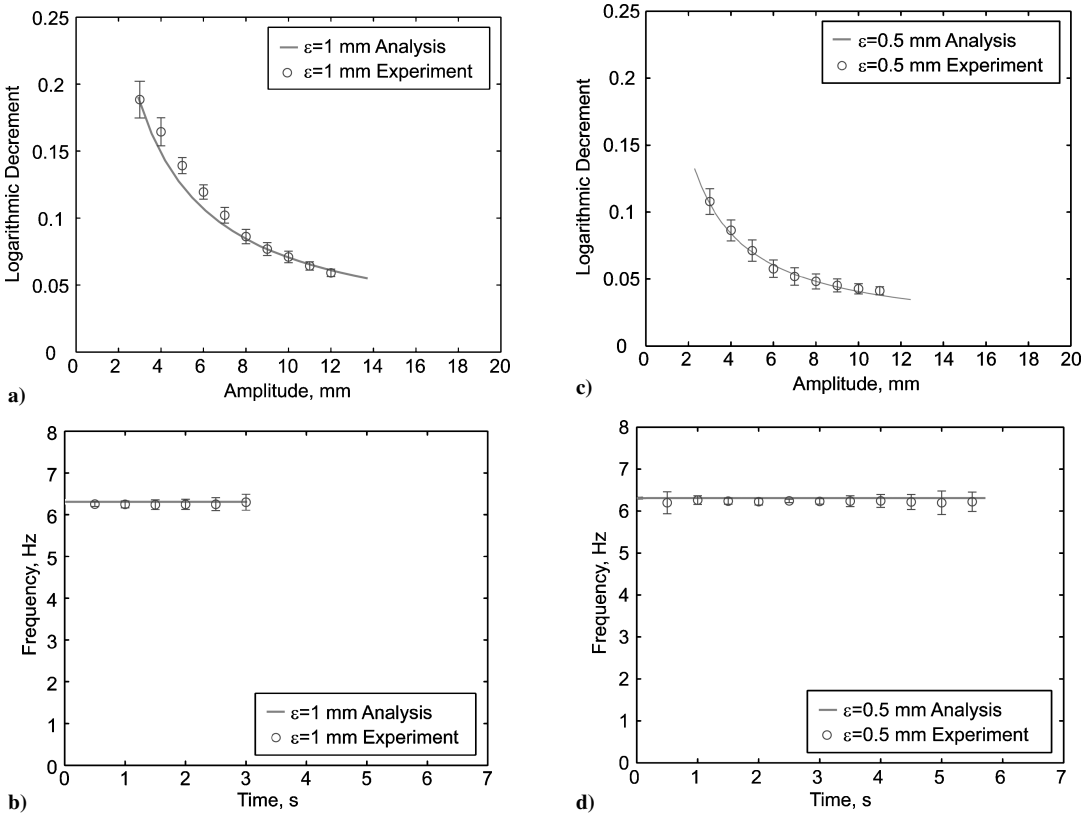

Fig. 16 Dynamic characteristics of configuration 2: a) logarithmic decrement, $\varepsilon = 1.0$ mm; b) time–frequency characteristics $\varepsilon = 1.0$ mm; c) logarithmic decrement, $\varepsilon = 0.5$ mm; and d) time–frequency characteristics, $\varepsilon = 0.5$ mm.

Figure 16 shows the results of configuration 2. It also shows that the proposed formulation provides very accurate estimations.

As shown in Figs. 14–16, the analyses can estimate these characteristics well, even though the dynamic characteristics in each condition were quite different. We confirmed that the proposed formulations are effective and applicable to the estimation of the dynamic characteristics of jointed structures.

The proposed formulations are useful for estimating not only the dynamic characteristic of space structures, but also new structural designs, such as no-prestress structures that meet the requirements. Furthermore, impact dampers[15–17] that dissipate vibration energy are an effective future application of the clearance effects seen here. Estimation of the clearance effects has the potential to permit the positive use of clearances as a damping element.

For multijointed structures, the proposed formulations are capable of predicting the dynamic characteristics. The frequency transition can be estimated in the same manner. The total energy loss can be calculated by summing each joint energy loss. A more detailed study of this will be the subject future work.

IV. Conclusions

Mathematical formulations were proposed to estimate the dynamic characteristics of free-vibrating structures that include joints. These formulations consist of a nonlinear spring model and friction- and impact-damping models. The friction models are mathematically formulated and simplified to make them easy to calculate. The impact damping models are formulated using the linear envelope of the time response. The dynamic characteristics can be estimated by integrating these models and formulations using the energy loss factors. This estimation is significantly more efficient than numerical simulations because the dynamic characteristics can be obtained immediately for each cycle using mathematical formulations. Analyses and experimental evaluations confirmed that the proposed formulations are valid and applicable to the dynamic characteristic estimation of jointed structures.

References

[1]Ueba, M., Ohata, K., Mitsugi, J., and Umehira, M., "Broadband and Scalable Mobile Satellite Communication System for Future Access Network," AIAA Paper 2004-3154, May 2004.

[2]Nurre, S. G., Ryan, S. R., Scofield, N. H., and Sims, L. J., "Dynamics and Control of Large Space Structures," *Journal of Guidance, Control, and Dynamics*, Vol. 7, No. 5, 1984, pp. 514–526.

[3]Ferri, A. A., "Modeling and Analysis of Nonlinear Sleeve Joints of Large Space Structures," *Journal of Spacecraft and Rockets*, Vol. 25, No. 5, 1988, pp. 354–360.

[4]Tzou, S. H., and Rong, Y., "Contact Dynamics of a Spherical Joint and a Jointed Truss-Cell System," *AIAA Journal*, Vol. 29, No. 1, 1991, pp. 81–88.

[5]Alexander, M. R., Noah, T. S., and Franck, G. C., "Parametric Identification of a Vibratory System with a Clearance," *Journal of Vibration and Acoustics*, Vol. 115, Jan. 1993, pp. 25–32.

[6]Aidanpaa, J. O., and Gupta, B. R., "Periodic and Chaotic Behavior of a Threshold-Limited Two-Degree-of-Freedom System," *Journal of Sound and Vibration*, Vol. 165, No. 2, 1993, pp. 305–327.

[7]Peterka, F., and Vacik, J., "Transition to Chaotic Motion in Mechanical Systems with Impacts," *Journal of Sound and Vibration*, Vol. 154, No. 1, 1992, pp. 95–115.

[8]Crawley, F. E., and O'Donnell, J. K., "Force-State Mapping Identification of Nonlinear Joints," *AIAA Journal*, Vol. 25, No. 7, 1987, pp. 1003–1010.

[9]Folkman, L. S., and Redd, J. F., "Gravity Effects on Damping of a Space Structure with Pinned Joints," *Journal of Guidance, Control, and Dynamics*, Vol. 13, No. 2, 1990, pp. 228–233.

[10]Folkman, L. S., Bingham, G. J., Crookston, R. J., Dutson, D. J., Fernery, D. B., Ferney, D. G., and Rowsell, A. E., "The Joint Damping Experiment (JDX)," NASA CR 4781, June 1997.

[11]Blanchard, L., "A Prediction Method of Bolted Junction Microslip in High Stability Space Structures," International Astronautical Federation, 55th International Astronautical Congress, Paper IAC-04-I.1.01, Oct. 2004.

[12]Shibata, H., Amano, A., and Takada, H., "A New Semi-Numerical Approach on Response of Beam with Multi-Gaps and Its Chaotic Response," *Component Analysis and Evaluation, Aging and Maintenance, and Pipe Supports*, Vol. 376, *Proceedings of ASME/JSME Pressure Vessels and Piping Conference*, American Society of Mechanical Engineers, 1998, pp. 185–190.

[13]Foale, S., and Bishop, R. S., "Transient Response of a Constrained Beam Subjected to Narrow-Band Random Excitation," *Journal of Sound and Vibration*, Vol. 185, No. 4, 1995, pp. 723–733.

[14]Hachkowski, R. M., Peterson, D. L., and Lake, S. M., "Load Path Management Design Theory for Precision Deployable Joints," AIAA Paper 2000-1364, April 2000.

[15]Grubin, C., "On the Theory of the Acceleration Damper," *Journal of Applied Mechanics*, Vol. 23, Sept. 1956, pp. 373–378.

[16]Masri, F. S., and Caughey, K. T., "On the Stability of the Impact Damper," *Journal of Applied Mechanics*, Vol. 33, No. 3, 1966, pp. 586–592.

[17]Ma, S., and Semercigil, E. S., "A Modified Passive Tuned Absorber for Secondary Systems Under Random Excitation," *Journal of Sound and Vibration*, Vol. 208, No. 3, 1997, pp. 349–366.

L. Peterson
Associate Editor